

Article

An Effective Design Scheme of Single- and Dual-Band Power Dividers for Frequency-Dependent Port Terminations

Rahul Gupta ¹, Maher Assaad ², Muhammad Akmal Chaudhary ² and Mohammad Hashmi ^{3,*}

¹ ECE Department, Indraprastha Institute of Information Technology Delhi, New Delhi 110020, India; rahul@iiitd.ac.in

² Department of Electrical and Computer Engineering, College of Engineering and Information Technology, Ajman University, Ajman P.O. Box 346, United Arab Emirates; m.assaad@ajman.ac.ae (M.A.); m.akmal@ajman.ac.ae (M.A.C.)

³ Department of Electrical and Computer Engineering, School of Engineering and Digital Sciences, Nazarbayev University, Astana 010000, Kazakhstan

* Correspondence: mohammad.hashmi@nu.edu.kz; Tel.: +7-7172-706146

Abstract: Flexible design schemes for single- and dual-band power dividers terminated in arbitrary port impedances are proposed in this paper. The proposed architecture provides the inherent impedance transformation to real, complex, and frequency-dependent complex impedances at the input and output port terminations. Furthermore, the proposed design is supported by flexible design procedures with independent design variables to enhance rapid prototyping in microstrip technology. It is demonstrated that the presence of independent design variables enhances the design flexibility for varied ranges of frequency and impedance transformation ratios. Two different prototypes, one each demonstrating single- and dual-band performances, are developed to validate the performance of the reported designs with real and frequency-dependent complex port impedances. The prototypes exhibit excellent agreements between the simulated and measured results. The single-band impedance transforming power divider (ITPD) possesses a low-amplitude imbalance of 0.5 dB, a phase imbalance of less than $\pm 0.5^\circ$, and an isolation of -26 dB at the design frequency of 5.8 GHz. The dual-band prototype also exhibits a low-amplitude imbalance of 0.5 dB and a phase imbalance of less than $\pm 0.5^\circ$ at both the design frequencies of 1 GHz and 2.6 GHz. The isolation is also better than -30 dB at both design frequencies. It is thus shown that the overall performance advances the state of the art in the design schemes of ITPDs.

Keywords: Wilkinson power divider; design flexibility; frequency-dependent complex impedance transformation



Citation: Gupta, R.; Assaad, M.; Chaudhary, M.A.; Hashmi, M. An Effective Design Scheme of Single- and Dual-Band Power Dividers for Frequency-Dependent Port Terminations. *Electronics* **2023**, *12*, 1991. <https://doi.org/10.3390/electronics12091991>

Academic Editor: Reza K. Aminieh

Received: 9 March 2023

Revised: 9 April 2023

Accepted: 20 April 2023

Published: 25 April 2023



Copyright: © 2023 by the authors. Licensee MDPI, Basel, Switzerland. This article is an open access article distributed under the terms and conditions of the Creative Commons Attribution (CC BY) license (<https://creativecommons.org/licenses/by/4.0/>).

1. Introduction

There has been tremendous growth in wireless-related applications in the past decade, and this has necessitated the development of a variety of RF circuits and components operating at single or multiple frequencies simultaneously [1–15]. In this context, it is imperative to note that the design schemes for the Wilkinson power divider (WPD) have also seen rapid advances to support the requirements of wireless communication systems (WCS) [16–25]. For example, multiband WPD architectures are suitable for applications requiring operations at distant bands [26–34]. Furthermore, power dividers (PDs) operating at single/multiple frequencies with inherent impedance transformations for different types and levels of impedances are extremely advantageous [35–37]. Such architectures with inherent features have become compact and cost-effective.

In general, a number of PD design reports are available in the literature, which discuss the realization schemes for multifrequency operation (in terms of frequency ratio r) and impedance transformation (in terms of k) [16,19,22–24] with perhaps limited usefulness, emanating from complex design schemes, nonplanar architecture, incorporated reactive

elements, variable nature of impedance environments at the ports, dual–band operation, etc. Here, the frequency ratio (r) is referred as the ratio of higher design frequency (f_2) to lower design frequency (f_1), and the impedance transformation ratio (k) is the ratio of load/output impedance (Z_L) to source/input impedance (Z_S). The impedance transformation in a PD with dual–band operation is also reported, but the high-impedance transformation requirements are still elusive [22]. The relatively recent designs are either limited in achievable k or r [23,24]. Additionally, the design in [24] utilizes an admittance inverter to replace the conventional transmission lines (TL), which results in a large architecture. Moreover, there is absence of measurement validation of the impedance transformation [24]. In addition, most of the reported design schemes related to dual–band impedance-transforming power dividers (ITPDs) only talk about ports terminated in real impedances. There is one recent report that emphasizes the dual–band performance of the frequency-dependent complex impedance-transforming power divider, which utilizes the T-type impedance transformer at the ports [37]. Unfortunately, dual–band PDs with a varied nature of impedance environments at their respective ports are rare. It is thus clear that there is an emergent need for the design and performance evaluation of PDs under a varied nature of port impedances with the benchmarking of isolation, amplitude, and phase performance.

The proposed PD architecture in this paper therefore provides an inherent impedance transformation for single–/dual–band operations. The proposed design provides an analytical solution to enhance the operation of single–band equal port WPDs to arbitrary impedance environments at the ports at two arbitrary frequencies of operations. The proposed design is also augmented with independent design variables, which enhances the design flexibility further to provide high k and r simultaneously.

The design analysis of the proposed architecture is described in detail for both the single– and dual–band operations in Section 2. Section 3 illustrates the flexibility that the proposed design offers in terms of r and k . Finally, the proposed circuit is validated through two prototypes on single– and dual–band operations, each in Section 4. Section 5 follows with the conclusion.

2. Proposed Circuit and Design Analysis with Closed-Form Design Equations

The architecture of the proposed ITPD is shown in Figure 1. All the TLs are marked with respective characteristic impedances and electrical lengths. It should be noted here that the characteristic impedances are real and positive. This condition will also be helpful later in the design analysis. The input port (port 1) of the proposed power divider is terminated with the impedance Z_S (in Ω), and the output ports (ports 2 and 3) are each terminated with the impedance Z_L (in Ω). Both the port impedances, i.e., Z_S and Z_L , can either be a real, a complex, or an uncorrelated frequency-dependent complex load (FDCL). It is imperative to mention here that the output ports should have equal port impedances for the equal power division. To demonstrate both the real and complex environment in the design analysis of the proposed ITPD, Z_S is considered an arbitrary real impedance, while Z_L is an arbitrary complex impedance for the single–band operation and an arbitrary FDCL for the dual–band operation. The Z_L as an arbitrary FDCL is defined in (1) at the two arbitrary design frequencies f_1 GHz and f_2 GHz for dual–band operation. Here, $f_2 > f_1$ ($r = f_2/f_1$). Characteristic impedance (in Ω) and electrical length (in $^\circ$), defined at f_1 , of all the respective TL sections are depicted in Figure 1.

$$Z_L = \begin{cases} R_{L1} + jX_{L1} @f_1 \\ R_{L2} + jX_{L2} @f_2 \end{cases} \quad (1)$$

2.1. Design Analysis of the Single–Band ITPD

In this section, the proposed PD is analyzed for its operation at a single frequency, i.e., f_1 only. Owing to the symmetry of the architecture, odd–even mode analysis is provided to deduce the design equations. The respective odd- and even-mode equivalent circuits

are shown in Figures 2 and 3, respectively. The load impedance Z_L is a complex entity, i.e., $Z_L = R_{L1} + jX_{L1}$ for the single-band of operation.

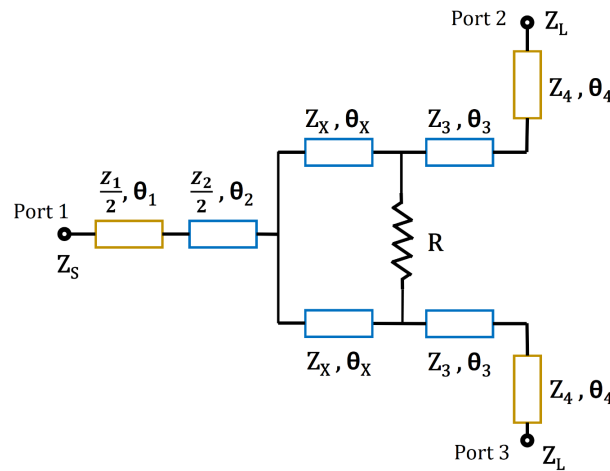


Figure 1. Proposed impedance-transforming single- and dual-band power divider circuit for real, complex, and FDCL port impedances.

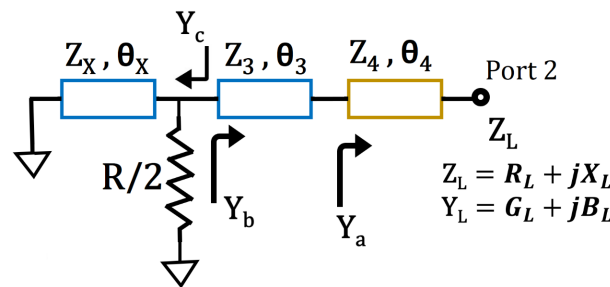


Figure 2. Odd-mode equivalent circuit for single-band operations.

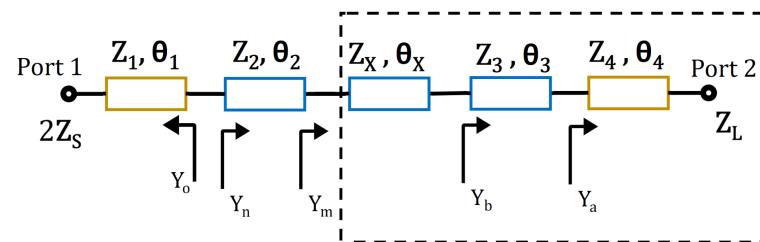


Figure 3. Even-mode equivalent circuit for single-band operations.

2.1.1. Odd-Mode Design Analysis

The odd-mode equivalent circuit of the proposed PD is shown in Figure 2. The input admittances Y_a , Y_b , and Y_c , derived using standard TL theory [38], are expressed in (2)–(4), respectively. For the impedance matching of the circuit, (5) must be followed to derive the expressions of R and Z_X . Here, the terms Z_3 , Z_4 , and all the electrical lengths are considered as the independent design variables, which makes the design scheme highly flexible for arbitrary port terminations. Subsequently, the term Y_b becomes a known quantity, which is expressed as $G_b + jB_b$. Following (5), the expressions of R and Z_X can be derived as (6) and (7), respectively. It should be recalled that the parameters R and Z_X are real and positive.

$$Y_a = \frac{Z_4 + j\frac{1}{Y_L} \tan\theta_4}{Z_4 \left(\frac{1}{Y_L} + jZ_4 \tan\theta_4 \right)} \tag{2}$$

$$Y_b = \frac{Z_3 + j\frac{1}{Y_a} \tan\theta_3}{Z_3 \left(\frac{1}{Y_a} + jZ_3 \tan\theta_3 \right)} = G_b + jB_b \quad (3)$$

$$Y_c = \frac{2}{R} + \frac{1}{jZ_X \tan\theta_X} \quad (4)$$

$$[Y_b] = [Y_c^*] \quad (5)$$

$$R = \frac{2}{G_b} \quad (6)$$

$$Z_X = \frac{1}{B_b \tan\theta_X} \quad (7)$$

2.1.2. Even-Mode Design Analysis

The even-mode equivalent circuit of the proposed ITPD is shown in Figure 3. The design parameters Z_X , Z_3 , Z_4 , θ_X , θ_3 , and θ_4 are known from the odd-mode analysis. Now, using standard TL theory [38], the admittances Y_m , Y_n , and Y_o can be expressed in (8)–(10), respectively. Again, for the impedance matching, (11) should be invoked to deduce the expressions of the design parameters Z_1 and Z_2 . The electrical lengths θ_1 and θ_2 are independent variables here, which further enhances the design flexibility. For the simpler design analysis, θ_1 and θ_2 can also be considered equal.

$$Y_m = \frac{Z_X + j\frac{1}{Y_b} \tan\theta_X}{Z_X \left(\frac{1}{Y_b} + jZ_X \tan\theta_X \right)} \quad (8)$$

$$Y_n = \frac{Z_2 + j\frac{1}{Y_m} \tan\theta_2}{Z_2 \left(\frac{1}{Y_m} + jZ_2 \tan\theta_2 \right)} \quad (9)$$

$$Y_o = \frac{Z_1 + j\frac{1}{2Y_S} \tan\theta_1}{Z_1 \left(\frac{1}{2Y_S} + jZ_1 \tan\theta_1 \right)} \quad (10)$$

$$[Y_o] = [Y_n^*] \quad (11)$$

A design flowchart of the proposed ITPD for the single-band operation is depicted in Figure 4. The presence of the independent design variables should be noted in the design procedure, as this enhances the design flexibility. The flexibility does not only make the design realizable for arbitrary port impedances, but choosing smaller values of θ_1 , θ_2 , θ_3 , θ_4 , and θ_X provides a compact design of the proposed ITPD. To clarify further, a numerical example can be assumed with $Z_S = 50 \Omega$ and $Z_L = 155.9 - j27 \Omega$ at the operating frequency of 1 GHz. Using (6) and (7), R and Z_X can be calculated as 50Ω and 38.5Ω , respectively, for the independent variables $Z_3 = 58.1 \Omega$, $\theta_3 = 65.5^\circ$, $Z_4 = 68.7 \Omega$, $\theta_4 = 13.6^\circ$, $\theta_X = 60^\circ$. Please note that if the calculated value of Z_X is not realizable within microstrip technology, i.e., $[20 \ 150] \Omega$, the independent variables can be chosen differently. Similarly, Z_1 and Z_2 can be calculated as 63.6Ω and 32.6Ω following (11) respectively, for the independently chosen $\theta_1 = 69.5^\circ$ and $\theta_2 = 73.3^\circ$. Again, the values of θ_1 and θ_2 can be chosen differently if Z_1 and Z_2 are not realizable within microstrip technology.

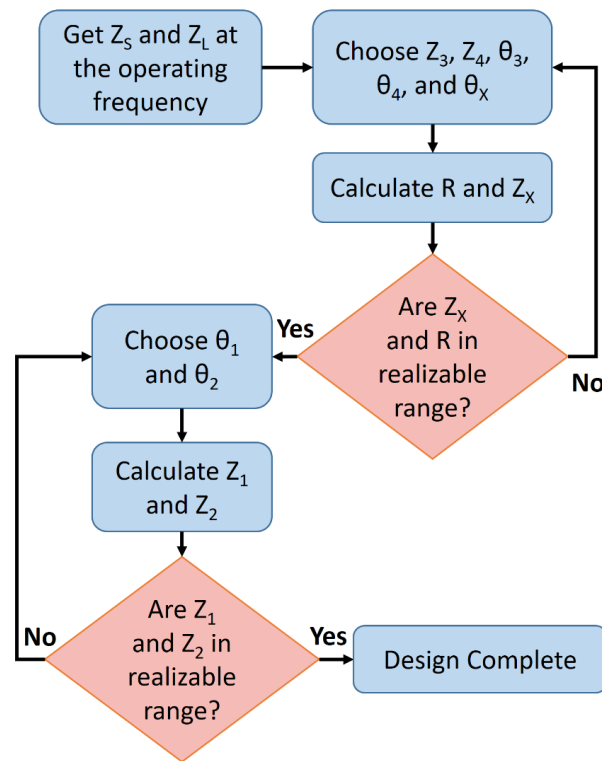


Figure 4. Design flowchart for the single–band ITPD.

2.2. Design Analysis of the Dual–Band ITPD

The proposed ITPD is also analyzed for its operation at two arbitrary design frequencies for the dual–band operation. Subsequently, the variation at the arbitrarily chosen design frequencies highlights the FDCL nature of the port impedances. The impedance Z_S is an arbitrary real impedance and Z_L is an arbitrary FDCL (1).

2.2.1. Odd-Mode Design Analysis

The odd-mode equivalent circuit of the proposed ITPD for the dual–band operation is depicted in Figure 5. The arbitrary FDCL Z_L (or $1/Y_L$) is converted to a complex conjugate admittance Y_a for Z_4 and θ_4 , as expressed in (12) and (13), respectively [39].

$$Z_4 = \sqrt{R_{L1}R_{L2} + X_{L1}X_{L2} + \frac{X_{L1} + X_{L2}}{R_{L2} - R_{L1}} (R_{L1}X_{L2} - R_{L2}X_{L1})} \tag{12}$$

$$\theta_4 = \frac{\pi + \arctan \frac{Z_4(R_{L1} - R_{L2})}{R_{L1}X_{L2} - R_{L2}X_{L1}}}{1 + r}, \tag{13}$$

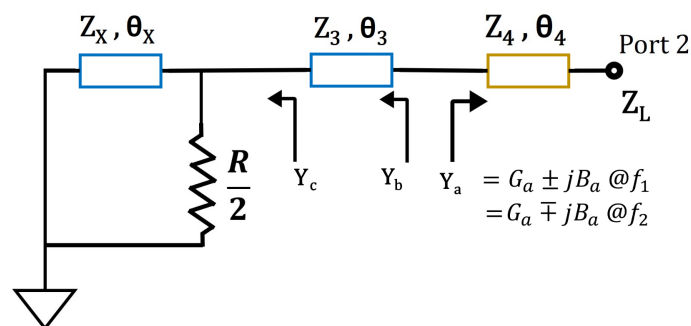


Figure 5. Odd-mode equivalent circuit for dual–band operations.

Subsequently, to achieve impedance matching for the odd-mode equivalent circuit, Y_b should follow (14), which results in the expressions of the design parameters Z_3 and Z_X . The electrical lengths are considered equal, i.e., $\theta_3 = \theta_X = \theta$, for the simplification of the expressions. The real and imaginary parts of the admittances Y_a and Y_b are expressed in (15), (16) and (17), (18), respectively. The admittance Y_b will also be a complex conjugate entity if θ follows (21) [40].

$$[Y_b] = [Y_a^*] \tag{14}$$

$$Re[Y_a] = G_a \tag{15}$$

$$Im[Y_a] = B_a \tag{16}$$

$$Re[Y_b] = \frac{2RZ_X^2 \tan^2 \theta (\tan^2 \theta + 1)}{A} \tag{17}$$

$$Im[Y_b] = \frac{R^2 Z_X^2 \tan^3 \theta (B)}{Z_3 A} \tag{18}$$

where

$$A = R^2 + \tan^2 \theta (R^2 Z_3^2 Z_X^2 \tan^2 \theta - 2R^2 Z_3 Z_X + 4Z_X^2) \tag{19}$$

$$B = \frac{4}{R^2} - Z_3^2 - \frac{Z_3}{Z_X} + \frac{Z_3}{Z_X \times \tan^2 \theta} + \frac{1}{Z_X^2 \times \tan^2 \theta} \tag{20}$$

$$\theta = \frac{(1+n)\pi}{1+r}; n \in (0, 1, 2, \dots) \tag{21}$$

2.2.2. Even-Mode Design Analysis

The even-mode equivalent circuit of the proposed power divider for the dual-band operation is shown in Figure 6. It is apparent from the circuit that except Z_1 and Z_2 , all the design parameters are already calculated in the odd-mode analysis. Therefore, the input impedance Z_m is known, and can be written as $R_m + jX_m @f_1$, and $R_m - jX_m @f_2$, where R_m and X_m are the real and imaginary parts of Z_m , respectively. Again, the electrical lengths are considered equal, i.e., $\theta_1 = \theta_2 = \theta$, as in (21), for the simplification of the expressions. Using standard TL theory [38], the expressions for impedances Z_n (22) and Z_o (23) can be deduced. Invoking $Z_o = 2Z_S$, and simplifying (22) and (23) provides Z_1 and Z_2 with $a = \tan \theta$ [41].

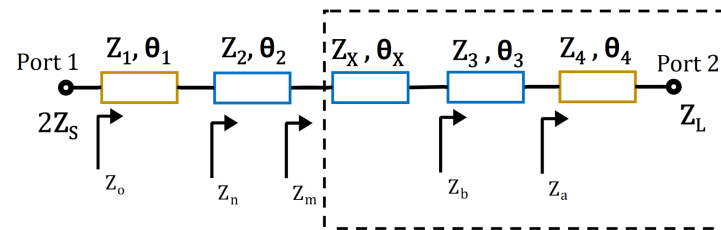


Figure 6. Even-mode equivalent circuit for dual-band operations.

$$Z_n = Z_2 \frac{Z_m + jZ_2 \tan \theta}{Z_2 + jZ_m \tan \theta} \tag{22}$$

$$Z_o = Z_1 \frac{Z_n + jZ_1 \tan \theta}{Z_1 + jZ_n \tan \theta} \tag{23}$$

$$2Z_S a^2 Z_2^2 + [2Z_S X_m a + Z_1 (R_m - 2Z_S)] Z_2 + [Z_1 2Z_S X_m a - Z_1^2 R_m a^2] = 0 \tag{24}$$

$$Z_1 a Z_2^2 + [Z_1 X_m - R_m 2 Z_S a + Z_1^2 a] Z_2 - [Z_1 2 Z_S R_m a + Z_1^2 X_m a^2] = 0 \quad (25)$$

A design flowchart of the proposed dual-band PD is depicted in Figure 7. It is apparent from the flowchart that the independent design parameters are reduced in comparison to the single-band ITPD, which is due to the additional burden of dual-band characteristics with the arbitrary frequency-dependent impedance transformation. The design parameter R is the only independent variable here. The electrical lengths must follow (21) for the dual-band operation of the impedance-transforming PD, except θ_4 , which is provided in (13). However, the design cases with real impedance terminations at the output ports θ_4 should also follow (21). Again, to further clarify the design procedure, a numerical example can be assumed with $Z_S = 30 \Omega$ and $Z_L = 54.14 + j8.6 \Omega$ at 1 GHz and $70.7 + j5.3 \Omega$ at 2.6 GHz. Using (12) and (13), Z_4 and θ_4 can be calculated to 60Ω and 70° , respectively. Now, (14) is used to calculate $Z_3 = 49.29 \Omega$ and $Z_X = 108.37 \Omega$ for independently chosen $R = 93 \Omega$, whereas (21) is used to calculate $\theta_3 = \theta_X = 50^\circ$. Please note that if the calculated values of Z_3 and Z_X are not realizable within microstrip technology, i.e., $[20 \text{ } 150] \Omega$, the independent variable R can be chosen differently. Now, Z_1 and Z_2 can be calculated to 62.34Ω and 33.22Ω using (24) and (25), respectively. and $\theta_1 = \theta_2$ are calculated to 50° using (21).

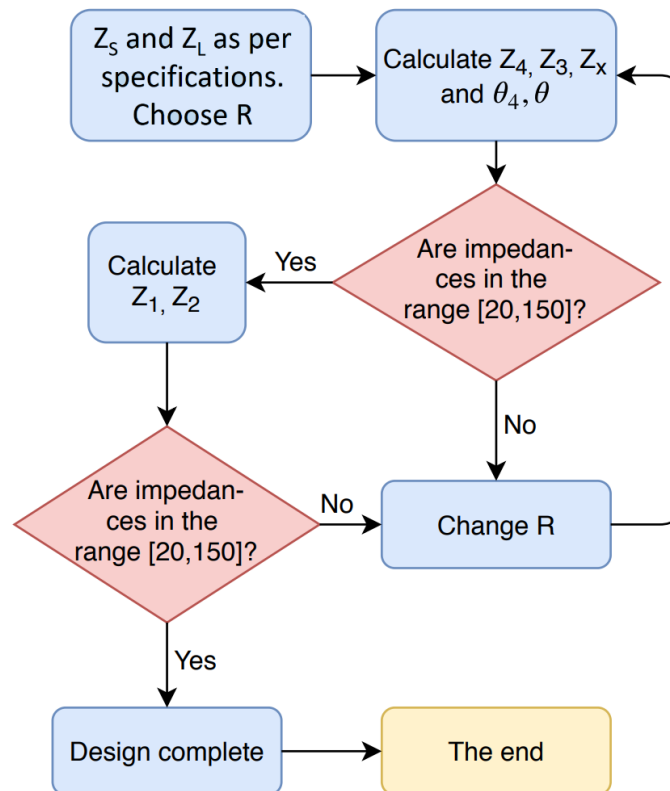


Figure 7. Design flowchart for the dual-band ITPD.

3. Case Studies

The proposed design of ITPD is an ideal solution for the varying impedance environments that are usually required in the front-end circuits of a wireless communication system. The effectiveness of the proposed design is studied by evaluating its design parameters for varied design specifications such as arbitrary port terminations and arbitrary design frequencies. The port terminations can independently be a real, complex, or FDCL in nature based on the design requirements.

It is apparent from the previous section that the design flexibility of the proposed ITPD is limited for the dual-band operation due to fewer independent design variables

in comparison to a single frequency of operation. It is, therefore, prudent to evaluate the range of k and r for the dual–band operation of the proposed ITPD.

3.1. Case Study: Frequency Ratios (R)

The proposed ITPD is capable of providing arbitrary r for the dual–band operation. To analyze the range of r , an arbitrary design example with input impedance (Z_S) = 50 Ω and output impedance (Z_L) = 50 Ω is selected. The minimum and maximum range of r is evaluated for the realizable design parameters. These calculated design parameters for distinct r are plotted in Figure 8, which reveals that all the design parameters ($Z_3, Z_X, Z_1/2, Z_2/2, Z_4$) are within the realizable range in microstrip technology [20 150]. For resistor R , it may take any value within or beyond [20 150] Ω , based on the manufacturer’s availability. A very wide range of r from 1.1 to 5.7 is achieved in this study. It should also be noted that the FDCL port terminations and their variations with frequency may influence the range of r , unlike the arbitrary but real port terminations.

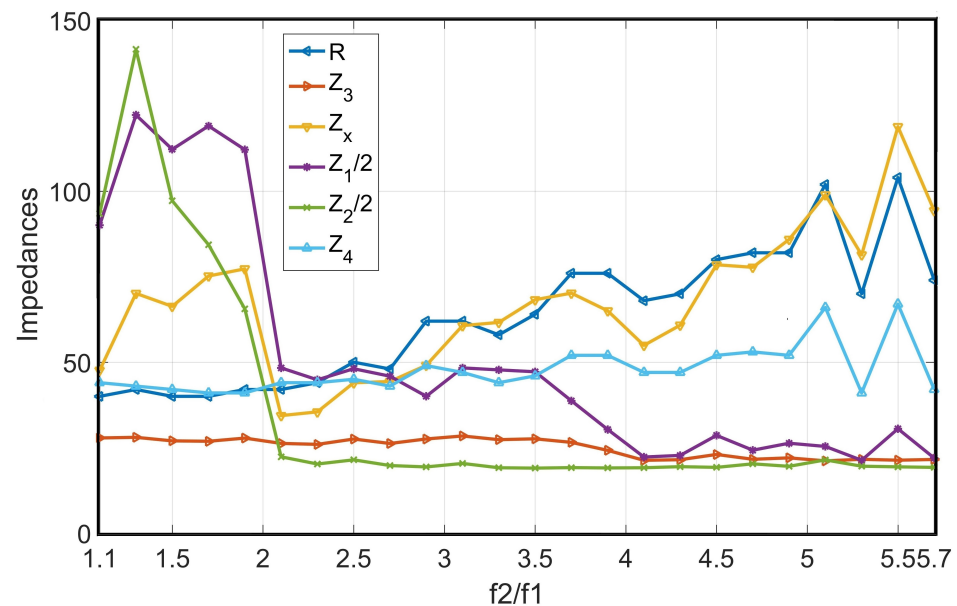


Figure 8. Design parameters for different frequency ratios for $Z_L = 50$ and $Z_S = 50$.

3.2. Case Study: Impedance Transformation Ratios (K)

In this case study, the proposed ITPD is evaluated for the range of k for a fixed value of $r = 2$. Again, the design parameters are calculated for the output port impedances $Z_L = 54.14 + j8.6@f_1$ GHz, and $Z_L = 70.6 + j5.3@f_2$ GHz. The frequency ratio is fixed at $r = 2$ and the source impedance Z_S is varied, from an impedance as low as 5 Ω to as high as 425 Ω . The respective design parameters are calculated and plotted in Figure 9. All the design parameters are realizable in microstrip technology [20 150]. This analysis demonstrates the effectiveness of the proposed ITPD for high impedance transformations while transforming an arbitrary real impedance to an arbitrary FDCL impedance. Additionally, the ITPD is also evaluated and plotted for the real port terminations in Figures 10 and 11. Here, the load impedances are fixed at 50 Ω , while the source impedance is varied, from as low as 5 Ω to as high as 600 Ω . For the clarity of the plots, Figures 10 and 11 are plotted separately to demonstrate the calculated design variables when the source impedance is lower and greater than Z_L , respectively. These plots convey that the proposed ITPD is an ideal choice for a very wide range of arbitrary r for real, complex, and FDCL port terminations at any port. The achievable k will significantly improve the single–band operation, considering the fact that the single–band ITPD possess enhanced design flexibility owing to a higher number of design variables.

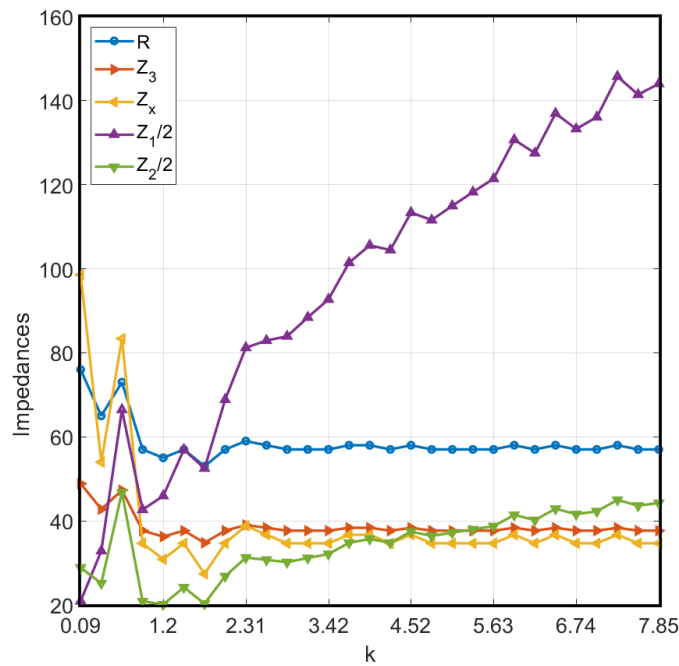


Figure 9. Design parameters for impedance ratios for $Z_L = 54.135 + j8.595@f_1; 70.656 + j5.269@f_2$ and $r = 2$ for $5 \Omega \leq Z_S \leq 425 \Omega$.

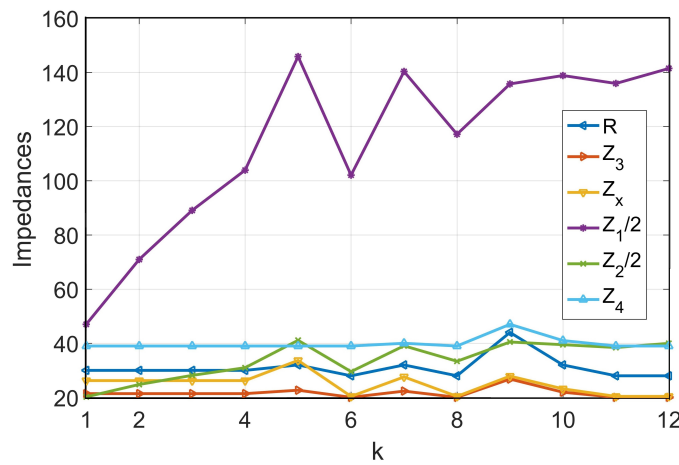


Figure 10. Design parameters for different impedance ratios for $Z_L = 50$ and $r = 2$ for $Z_S \geq Z_L$.

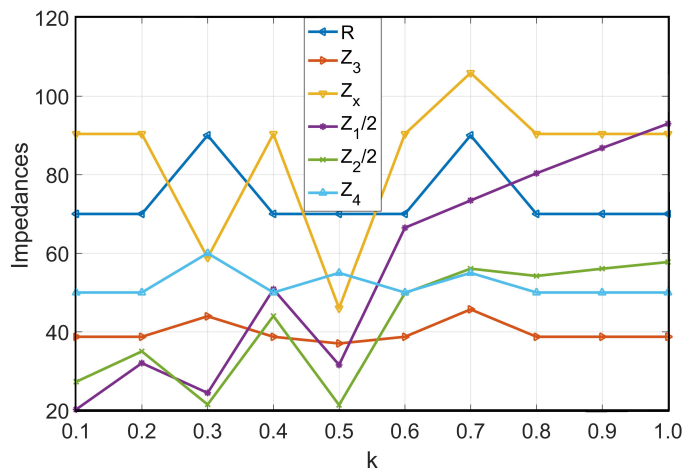


Figure 11. Design parameters for different impedance ratios for $Z_L = 50$ and $r = 2$ for $Z_S \leq Z_L$.

The design parameters for some of the design cases with arbitrary r and k are calculated and listed in Table 1. Case 1 depicts the design case with the dual–band operation of the ITPD for an FDCL impedance at the output ports. Cases 2 and 3 also demonstrate the design cases with FDCL impedance, but with different r and k . The design Cases 4 and 5 have real port impedances at all the ports with different r and k . Case 6 of Table 1 depicts the design parameters for the single–band operation of the proposed ITPD.

Table 1. Calculated values of the design parameters of the proposed ITPD [* based on the real part of the impedances at the ports, # single–band design case].

Case	r ($f_1 = 1$ GHz)	k^* @ f_1, f_2	Load $Z_L(\Omega)$	Z_S , (Ω)	$Z_1(\Omega)$, $\theta_1(^{\circ})$	$Z_2(\Omega)$, $\theta_2(^{\circ})$	$Z_3(\Omega)$, $\theta_3(^{\circ})$	$Z_4(\Omega)$, $\theta_4(^{\circ})$	$Z_X(\Omega)$, $\theta_X(^{\circ})$	$R(\Omega)$
1	2.6	0.55 0.42	$54.14 + j8.6 @ f_1$ $70.7 + j5.3 @ f_2$	30	62.34, 50	33.22, 50	49.29, 50	60, 70	108.37, 50	93
2	3	20, 8	$20 + j8 @ f_1$ $50 + j5 @ f_2$	400	94.4, 45	65.2, 45	28.9, 45	30.2, 63	60.1, 45	71
3	4.5	5, 2	$20 + j8 @ f_1$ $50 + j5 @ f_2$	100	45.73, 32.73	31.93, 32.73	20.96, 32.73	30.17, 45.76	105.51, 32.73	86
4	5	2, 2	$50 @ f_1$ $50 @ f_2$	100	30, 30	42.34, 30	22.4, 30	77, 30	110.9, 30	120
5	2	10, 10	$50 @ f_1$ $50 @ f_2$	500	138.8, 60	39.5, 60	21.9, 60	41, 60	23.2, 60	32
6	NA #	3.12	$155.9 - j27 @ f_1$ $155.9 - j27 @ f_2$	50	63.6, 69.5	32.6, 73.3	58.1, 65.5	68.7, 13.6	38.5, 60	50

3.3. Brief Discussion on Bandwidth Control

The proposed PD demonstrates a good improvement over the existing literature for the equal power division at arbitrary r and k . Considering the requirements from the practical design environment, the proposed ITPD is tested in a simulation setup for bandwidth improvement. Owing to the independent variables, the selection of the design parameters has the ability to provide reasonable improvements on the operational bandwidth. It has been identified that the bandwidth of the proposed ITPD can be controlled using Z_X and R . It is found that keeping Z_X and R at higher values increases the overall bandwidth of the PD. Furthermore, the variation in Z_X and R controls the isolation bandwidth up to a great extent. It has been seen that the higher Z_X leads to the increased outband isolation bandwidth, whereas a higher R improves the inband bandwidth. It is worthwhile to note that in cases of limited flexibility, Z_X should be prioritized over R for the higher operational bandwidth.

4. Fabrication and Experiment

The proposed ITPD is a good solution for the frequency-dependent impedance environments for single– or dual–band operations. To experimentally evaluate the performance of the proposed design, two different prototypes were fabricated on the microstrip technology. The first prototype demonstrates the single–band operation, which is designed at a high frequency of 5.8 GHz (WLAN), and the arbitrary output port impedance is $155.9-j27 \Omega$. The source impedance is fixed to the conventional 50Ω . The calculated design parameters for this design are mentioned in case 6 of Table 1. The prototype is fabricated on RO5880 substrate with a substrate thickness of 1.57 mm, a relative permittivity (ϵ_r) of 2.2, and a dissipation factor ($\tan \delta$) of 0.0009. The substrate has laminates of $35 \mu\text{m}$ thick copper on both the sides. The fabricated prototype is soldered with 50Ω isolation resistor (part no. CRCW060350R0FKEA), and is depicted in Figure 12. The dimensions of the single–band ITPD, without the encircled impedance transformers, are $38.6 \text{ mm} \times 17.6 \text{ mm}$. However, an L-type impedance transformer is added at the output ports to transform the complex

impedance to $50\ \Omega$ for the compatible measurement environment. Some optimizations in the design environment are performed using the industry standard electronic design automation (EDA) tool, i.e., Keysight ADS, to compensate for the anomaly associated with the resistor gap, junction discontinuities, bends, etc.

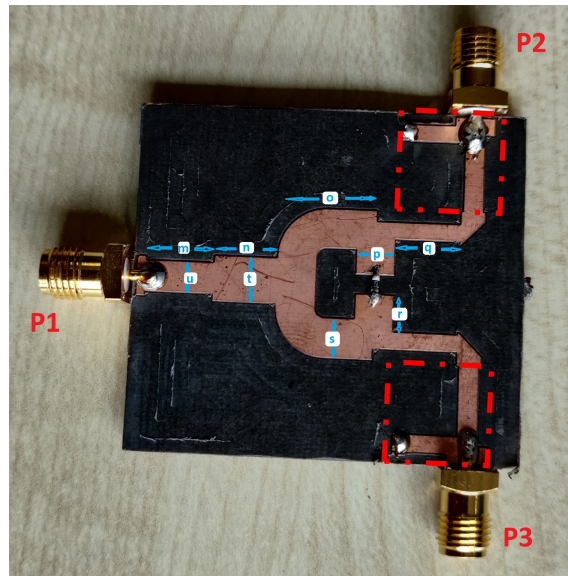


Figure 12. Prototype of single-band ITPD with impedance transformers at the output ports (encircled). P1/2/3 designates port 1/2/3 here. $m = 8.17\ \text{mm}$, $n = 7.74\ \text{mm}$, $o = 12.47\ \text{mm}$, $p = 4.73\ \text{mm}$, $q = 8.17\ \text{mm}$, $r = 3.9\ \text{mm}$, $s = 4.37\ \text{mm}$, $t = 5.2\ \text{mm}$, $u = 3.5\ \text{mm}$.

The measurement results of the prototype are depicted in Figures 13–15. The calculated results are also plotted for reference in Figure 16. Apparently, the measurement results (suffixed with M) and the EM-simulated results (suffixed with EM) are in good agreement. The input port matching and the isolation, as depicted in Figure 13, are better than $-26\ \text{dB}$ at the design frequency. The matching at the output ports (S_{22} and S_{33}) is depicted in Figure 14, and the insertion losses (S_{21} and S_{31}) and the phase difference between the two output ports are depicted in Figure 15, respectively. The 3 dB fractional bandwidth (FBW) is measured to be 65.5% for the slight amplitude imbalance of 0.5 dB. For the measured bandwidth, the phase imbalance is also very good and is within the tolerance of $\pm 0.5^\circ$. The amplitude imbalance is the magnitude difference between the output power at the output ports, whereas the phase imbalance is the deviation from the 0° phase difference between the output power at the output ports.

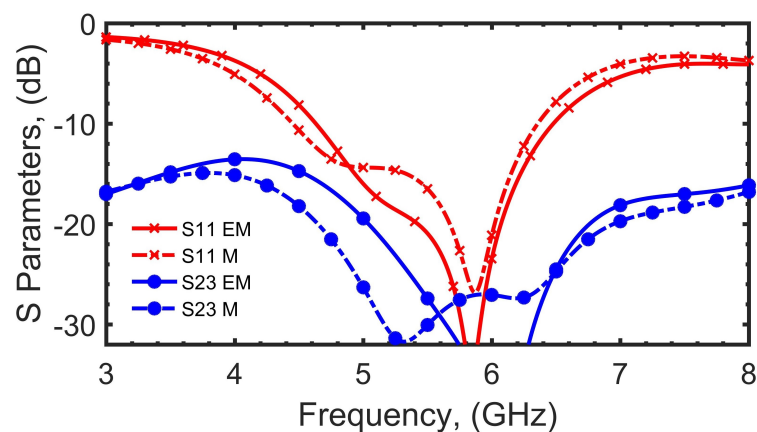


Figure 13. The EM simulation (EM) vs. measurement results (M) for S_{11} and S_{23} of the fabricated prototype for the single-band operation.

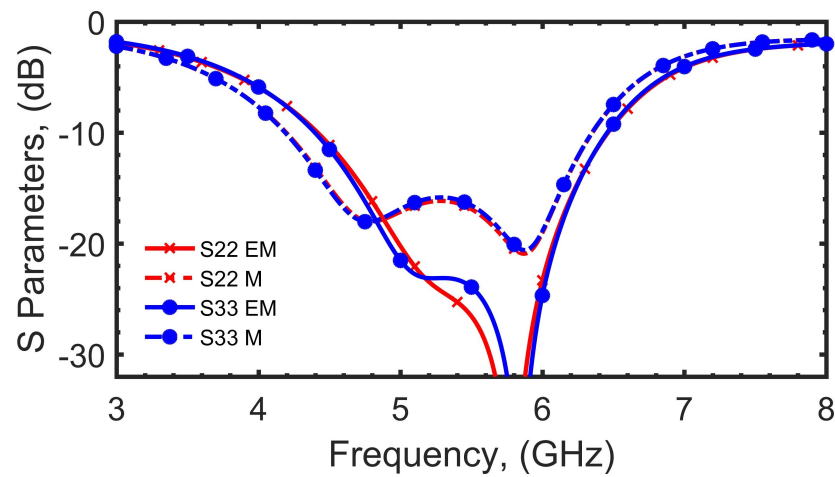


Figure 14. The EM simulation (EM) vs. measurement results (M) for S_{22} and S_{33} of the fabricated prototype for the single-band operation.

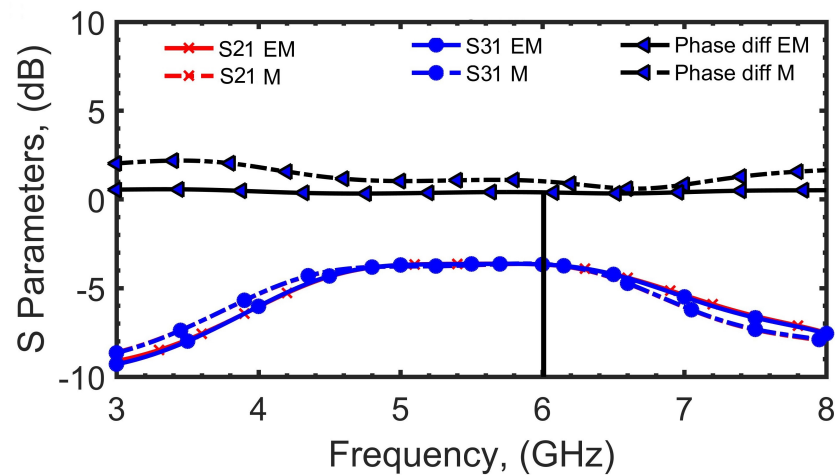


Figure 15. The EM simulation (EM) vs. measurement results (M) for S_{21} , S_{31} , and phase difference between the output ports of the fabricated prototype for the single-band operation.

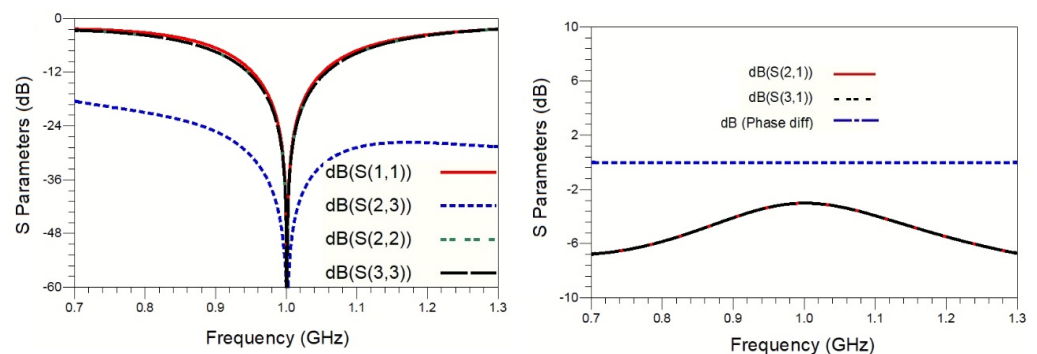


Figure 16. Calculated results of Case 6 for the single-band operation.

Subsequently, to demonstrate the effectiveness of the proposed ITPD at two arbitrary frequencies, another prototype working at 1 GHz and 2.6 GHz, and again with FDCL port impedances of $54.14 + j8.6 @ 1 \text{ GHz}$ and $70.7 + j5.3 @ 2.6 \text{ GHz}$, is developed. In this case, the impedance transformation is demonstrated in the input port too, and it is fixed at 30Ω . The calculated design parameters for this design are mentioned in Case 1 of Table 1. The prototype, shown in Figure 17, is fabricated on RO4003 substrate with a substrate thickness of 1.52 mm, a relative permittivity (ϵ_r) of 3.38, and a dissipation factor ($\tan \delta$) of 0.0027.

The substrate has laminates of 35 μm thick copper on both the sides. Here, the soldered resistor is a commercially available 100 Ω (part no. CRCW0603100RFKTA). Necessary optimizations are performed in the design environment to compensate for the anomaly associated with the resistor, resistor gap, junction discontinuities, bends, etc. Here, the FDCL impedances at the output ports (P2 and P3) are synthesized by a combination of a microstrip line of width 2.54 mm and length of 15.47 mm and a 50 Ω SMA connector; however, the source impedance is transformed to 50 Ω using two-section transmission lines [42]. The developed prototype has an overall size of 65.7 mm \times 61.5 mm, which includes the dimensions of the synthesized ports at the output ports and the impedance transformer at the source port. The measurement results of this dual-band prototype are depicted in Figures 18–20. The calculated results are also plotted for reference in Figure 21. The phase difference in Figure 20 at 2.6 GHz is measured to be 2.53 $^\circ$, which can be attributed to the soldering and fabrication losses. Ignoring this anomaly, the 3 dB fractional bandwidth (FBW) is noticeable, which is measured to be greater than 60% at both the design frequencies for the slight amplitude and phase imbalance of 0.5 dB and $\pm 0.5^\circ$, respectively.

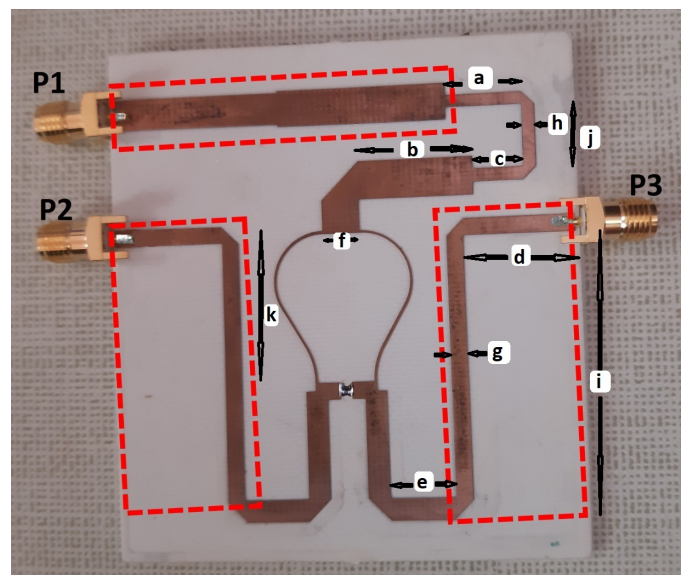


Figure 17. Prototype of the dual-band PD with impedance transformers at all the ports (encircled). $a = 11$ mm, $b = 16.4$ mm, $c = 7.13$ mm, $d = 15.4$ mm, $e = 8.7$ mm, $f = 4.8$ mm, $g = 2.4$ mm, $h = 2.3$ mm, $i = 40.28$ mm, $j = 7.6$ mm, $k = 21.28$ mm.

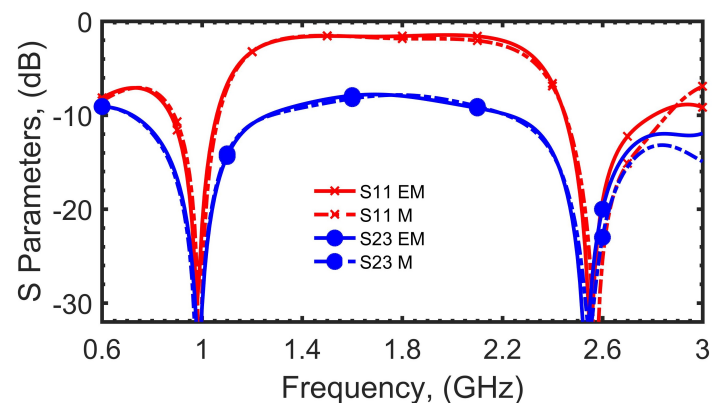


Figure 18. The EM simulation (EM) vs. measurement results (M) for S_{11} and S_{23} of the fabricated prototype for the dual-band operation.

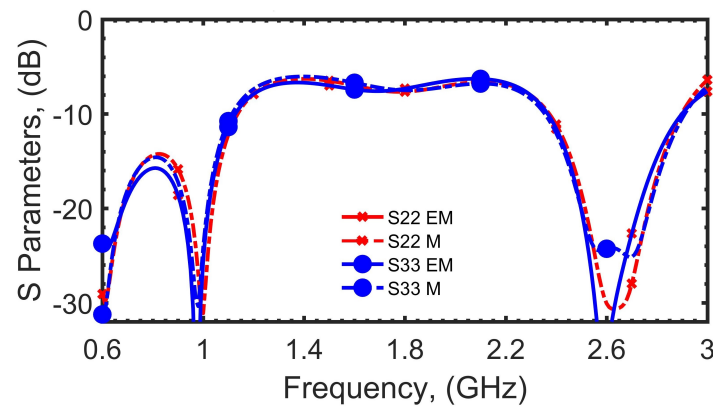


Figure 19. The EM simulation (EM) vs. measurement results (M) for S_{22} and S_{33} of the fabricated prototype for the dual-band operation.

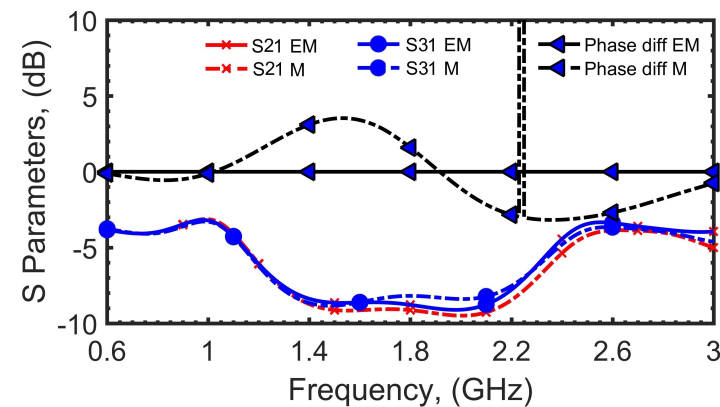


Figure 20. The EM simulation (EM) vs. measurement results (M) for S_{21} , S_{31} , and phase difference between the output ports of the fabricated prototype for the dual-band operation.

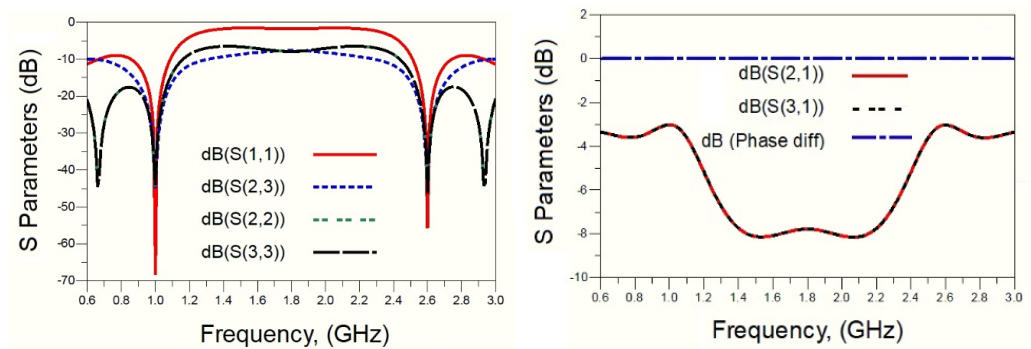


Figure 21. Calculated results of Case 1 for the dual-band operation.

In addition, the proposed ITPD is compared in terms of the number of bands, possible impedance transformations, fractional bandwidth, and the sizes with the recently reported PDs in Table 2. It was found that the impedance-transforming power dividers with inherent frequency-dependent complex impedance transformation are very limited in the literature. Either the power dividers provide frequency-dependent complex impedance transformation at a single frequency only, or only real impedance transformations at two arbitrary design frequencies. In comparison, the proposed power divider provides the real, complex, and frequency-dependent complex impedance transformation for single- and dual-band operations. Moreover, the proposed ITPD does not use any reactive element in the isolation circuit, irrespective of load impedances being real, complex, or FDCL. The size of these ITPDs is also of much importance for the compact size requirements. Though

the size of the single–band design is on the slightly higher side, this is due to fewer efforts on the suitable optimizations to achieve the compact design. However, additional efforts are made to keep the design favorably compact in the dual–band prototype, which is also apparent in the comparison table. It is also found that the proposed ITPD has superior amplitude and phase imbalance performance over most published state-of-the-art designs, such as [13,17,21,40]. Clearly, as demonstrated in Tables 1 and 2, the achievable r and k with the proposed ITPD is superior among the earlier published ITPDs, whether operating at single– or dual–band, which also demonstrates the high microstrip compatibility of the proposed design.

Table 2. Qualitative comparison with state-of-the-art impedance transforming power dividers [R: resistor, # 15 dB bandwidth, ## 20 dB bandwidth, * calculated/estimated from provided data].

Refs	No. of Bands	Impedance Transformation	Operating Frequencies (GHz)	S_{11} (dB) at f_1, f_2	S_{21} (dB) at f_1, f_2	S_{31} (dB) at f_1, f_2	FBW (%) at f_1, f_2	Size (λ_g^2)
[13]	single	-	1.5	-26 *	-3.27	-3.28	26.8 #	0.023
[43]	dual	-	1.0, 2.0	<-20	-3.7 *	-3.7 *	84.5	0.26
[44]	dual	-	2.4, 3.5	<-20	-3.94	-3.77	2.9 #, 8.6 #	0.095
[45]	dual	-	2.4, 3.5	<-20	-3.94	-3.77	10 ##, 5.5 ##	0.122
[20]	dual	-	1, 3.5	-20.0, -20.3	-3.28, -3.35	-3.25, -3.37	50 #, 15 #	0.023
[21]	dual	-	0.7, 2.6	<-15	-3.42, -4.96	-3.43, -1.94	24.3, 8.1	0.34
[18]	single	real	1	-31	-3.28	-3.42	8	0.088
[17]	single	complex	2.0	-29	-3.77	-3.38	36	0.35
[6]	single	complex	2	-17.5	-3.25	-3.25 *	16.8	0.25 *
[24]	dual	real	1, 6.4	<-30	-3.45, -4.37	-3.45, -4.37	53, 7.3	0.087 *
[40]	dual	real	1, 5	-29, -21	-3.6, -3.9	-3.4, -4.1	11, 12	0.175
[37]	dual	real, complex, and FDCL	1, 2.6	-31.8, -27.9	-3.2, -3.6	-3.2, -3.6	16 and 13.1	0.106
[This work]	single	real, complex, and FDCL	5.8	-26.1	-3.6	-3.6	65.5	0.40
[This work]	dual	real, complex, and FDCL	1, 2.6	-28.9, -27.8	-3.15, -3.7	-3.27, -3.65	18.2, 17.3	0.096

5. Conclusions

A thorough study and investigation of a generalized ITPD for single– and dual–band operations has been reported in this paper. The unique part of the investigation includes a detailed discussion on the versatility of impedances at the ports for a wide range of arbitrary r and k . The design procedure of the reported ITPD exhibits independent design parameters that make the design scheme very flexible for the inherent impedance transformation. To demonstrate the effectiveness of the proposed ITPD, several case studies have been provided with varying r and k at different design conditions. Based on the proposed design procedure, two different prototypes have also been fabricated, each for a single–band and dual–band operation. The superior features of both prototypes demonstrate a significant contribution to the domain of advanced ITPD configurations.

Author Contributions: Conceptualization, R.G. and M.H.; methodology, R.G. and M.H.; software, R.G.; validation, R.G., M.A. and M.H.; formal analysis, R.G., M.A., M.A.C. and M.H.; investigation, R.G. and M.H.; resources, R.G. and M.H.; data curation, R.G., M.A., M.A.C. and M.H.; writing—original draft preparation, R.G., M.A. and M.A.C.; writing—review and editing, M.A., M.A.C. and M.H.; visualization, R.G. and M.H.; supervision, M.H.; project administration, M.H.; funding acquisition, M.A. and M.H. All authors have read and agreed to the published version of the manuscript.

Funding: This work was supported by the Collaborative Research Program (CRP) Grant Number 021220CRP0222 and Faculty Development Competitive Research Grant (FDCRG) Number 20122022FD4113 at Nazarbayev University.

Data Availability Statement: Not Applicable.

Conflicts of Interest: The authors declare no conflict of interest.

References

1. Saxena, A.; Hashmi, M.; Banerjee, D.; Chaudhary, M.A. Theory and Design of a Flexible Two-Stage Wideband Wilkinson Power Divider. *Electronics* **2021**, *10*, 2168. [[CrossRef](#)]
2. Gomez-Garcia, R.; Ghannouchi, F.M.; Carvalho, N.B.; Luong, H.C. Guest editorial advanced circuits and systems for CR/SDR applications. *IEEE Trans. Emerg. Sel. Top. Circuits Syst.* **2013**, *3*, 485–488. [[CrossRef](#)]
3. Al Shamaileh, K.; Dib, N.; Abushamleh, S. A dual-band 1:10 Wilkinson power divider based on multi-T-section characterization of high-impedance transmission lines. *IEEE Microw. Wirel. Compon. Lett.* **2017**, *27*, 897–899. [[CrossRef](#)]
4. Maktoomi, M.A.; Hashmi, M.S.; Yadav, A.P.; Kumar, V. A Generic Tri-Band Matching Network. *IEEE Microw. Wirel. Compon. Lett.* **2016**, *26*, 316–318. [[CrossRef](#)]
5. Su, Y.; Fan, Y.; Lin, X.Q.; Wu, K. Single-Layer Mode Composite Coplanar Waveguide Dual-Band Filter With Large Frequency Ratio. *IEEE Trans. Microw. Theory Tech.* **2020**, *68*, 2320–2330. [[CrossRef](#)]
6. Hallberg, W.; Özen, M.; Kuylenstierna, D.; Buisman, K.; Fager, C. A generalized 3-dB wilkinson power divider/combiner with complex terminations. *IEEE Trans. Microw. Theory Tech.* **2018**, *66*, 4497–4506. [[CrossRef](#)]
7. Maktoomi, M.A.; Hashmi, M.S. A coupled-line based L-section DC-isolated dual-band real to real impedance transformer and its application to a dual-band T-junction power divider. *Prog. Electromagn. Res. C* **2014**, *55*, 95–104. [[CrossRef](#)]
8. Banerjee, D.; Saxena, A.; Hashmi, M.S. A Novel Concept of Virtual Impedance for High Frequency Tri-Band Impedance Matching Networks. *IEEE Trans. Circuits Syst. II* **2018**, *65*, 1184–1188. [[CrossRef](#)]
9. Maktoomi, M.A.; Hashmi, M.S.; Ghannouchi, F.M. A Dual-Band Port-Extended Branch-Line Coupler and Mitigation of the Band-Ratio and Power Division Limitations. *IEEE Trans. Comp. Manf. Tech.* **2017**, *7*, 1313–1323. [[CrossRef](#)]
10. Nguyen, N.; Ghiotto, A.; Martin, T.; Vilcot, A.; Wu, K.; Vuong, T. A 90° Self-Compensating Slab Air-Filled Substrate Integrated Waveguide Phase Shifter. In Proceedings of the IEEE MTT-S International Microwave Symposium (IMS), Boston, MA, USA, 2–7 June 2019; pp. 580–583. [[CrossRef](#)]
11. Guo, J.; Wu, K. Mode composite waveguide directional coupler. In Proceedings of the 2018 IEEE MTT-S International Wireless Symposium (IWS), Chengdu, China, 6–10 May 2018; pp. 1–4. [[CrossRef](#)]
12. Maktoomi, M.A.; Gupta, R.; Hashmi, M.S. A dual-band impedance transformer for frequency-dependent complex loads incorporating an L-type network. In Proceedings of the 2015 Asia-Pacific Microwave Conference (APMC), Nanjing, China, 6–9 December 2015; pp. 1–3. [[CrossRef](#)]
13. Xia, B.; Cheng, J.; Wu, L.; Xiong, C.; Mao, J. A new compact power divider based on capacitor central loaded coupled microstrip Line. *IEEE Trans. Microw. Theory Tech.* **2020**, *68*, 4249–4256. [[CrossRef](#)]
14. Maktoomi, M.A.; Gupta, R.; Maktoomi, M.H.; Hashmi, M.S.; Ghannouchi, F.M. A generalized multi-frequency impedance matching technique. In Proceedings of the 2016 16th Mediterranean Microwave Symposium (MMS), Abu Dhabi, United Arab Emirates, 14–16 November 2016; pp. 1–4. [[CrossRef](#)]
15. Maktoomi, M.A.; Hashmi, M.S.; Ghannouchi, F.M. Systematic Design Technique for Dual-Band Branch-Line Coupler Using T- and Pi-Networks and Their Application in Novel Wideband-Ratio Crossover. *IEEE Trans. Compon. Packag. Manuf. Technol.* **2016**, *6*, 784–795. [[CrossRef](#)]
16. Kim, P.; Chaudhary, G.; Jeong, Y. Analysis and design of an unequal termination impedance power divider with bandpass filtering response. *IET Electron. Lett.* **2017**, *53*, 1260–1262. [[CrossRef](#)]
17. Wu, Y.; Zhuang, Z.; Jiao, L.; Liu, Y. A novel balanced-to-unbalanced complex impedance-transforming in-phase power divider. *IEEE Access* **2017**, *5*, 205–213. [[CrossRef](#)]
18. Gupta, R.; Hashmi, M.S. High impedance transforming simplified balun architecture in microstrip technology. *Wiley Microw. Opt. Technol. Lett.* **2018**, *60*, 3019–3023. [[CrossRef](#)]
19. Wu, Y.; Zhuang, Z.; Kong, M.; Jiao, L.; Liu, Y.; Kishk, A.A. Wideband filtering unbalanced-to-balanced independent impedance-transforming power divider with arbitrary power ratio. *IEEE Trans. Microw. Theory Tech.* **2018**, *66*, 4482–4496. [[CrossRef](#)]

20. Liu, F.; Lee, J. Design of new dual-band wilkinson power dividers with simple structure and wide isolation. *IEEE Trans. Microw. Theory Tech.* **2019**, *67*, 3628–3635. [[CrossRef](#)]
21. Zaidi, A.M.; Beg, M.T.; Kanaujia, B.K.; Mainuddin; Rambabu, K. A compact dual-band out of phase power divider having microstrip compatibility. *IEEE Trans. Circuits Syst. II Exp. Briefs* **2020**, *67*, 2998–3002. [[CrossRef](#)]
22. Zhang, W.; Ning, Z.; Wu, Y.; Yu, C.; Li, S.; Liu, Y. Dual-band out-of-phase power divider with impedance transformation and wide frequency ratio. *IEEE Microw. Wirel. Compon. Lett.* **2015**, *25*, 787–789. [[CrossRef](#)]
23. Zhang, W.; Wu, Y.; Yu, C.; Li, S.; Wang, W.; Su, M.; Liu, Y. Dual band balanced-to-unbalanced power divider with inherent impedance transformation. *Electromagnetics* **2017**, *37*, 127–137. [[CrossRef](#)]
24. Zhuang, Z.; Wu, Y.; Kong, M.; Wang, W.; Liu, Y. Dual-band filtering balanced-to-unbalanced impedance-transforming power divider with high frequency ratio and arbitrary power division. *IEEE Access* **2018**, *6*, 12710–12717. [[CrossRef](#)]
25. Maktoomi, M.A.; Hashmi, M.S. A Performance Enhanced Port Extended Dual-Band Wilkinson Power Divider. *IEEE Access* **2017**, *5*, 11832–11840. [[CrossRef](#)]
26. Li, Y.; Sim, C.; Luo, Y.; Yang, G. 12-Port 5G massive MIMO antenna array in sub-6ghz mobile handset for LTE bands 42/43/46 applications. *IEEE Access* **2018**, *6*, 344–354. [[CrossRef](#)]
27. Li, H.; Miers, Z.T.; Lau, B.K. Design of orthogonal MIMO hand-set antennas based on characteristic mode manipulation at frequency bands below 1 GHz. *IEEE Trans. Antennas Propag.* **2014**, *62*, 2756–2766. [[CrossRef](#)]
28. Zhu, Y.; Zheng, G.; Wang, L.; Wong, K.; Zhao, L. Content placement in cache-enabled sub-6 ghz and millimeter-wave multi-antenna dense small cell networks. *IEEE Trans. Wirel. Commun.* **2018**, *17*, 2843–2856. [[CrossRef](#)]
29. Gu, X.; Srinaga, N.N.; Guo, L.; Hemour, S.; Wu, K. Diplexer-based fully passive harmonic transponder for sub-6-ghz 5G-compatible IoT applications. *IEEE Trans. Microw. Theory Tech.* **2019**, *67*, 1675–1687. [[CrossRef](#)]
30. Zahra, M.; Kempf, I.; Haarla, J.; Antonov, Y.; Khonsari, Z.; Miilunpalo, T.; Ahmed, N.; Inkinen, J.; Unnikrishnan, V.; Lehtovuori, A.; et al. A 2-5.5 ghz beamsteering receiver IC with 4-element vivaldi antenna array. *IEEE Trans. Microw. Theory Tech.* **2020**, *68*, 3852–3860. [[CrossRef](#)]
31. Liu, Y.; Li, C.; Xia, X.; Quan, X.; Liu, D.; Xu, Q.; Pan, W.; Tang, Y.; Kang, K. Multiband user equipment prototype hardware design for 5G communications in sub-6-ghz band. *IEEE Trans. Microw. Theory Tech.* **2019**, *67*, 2916–2927. [[CrossRef](#)]
32. Huang, M.; Lin, Y.L.; Ou, J.-H.; Zhang, X.Y.; Lin, Q.W.; Che, W.; Xue, Q. Single- and dual-band RF rectifiers with extended input power range using automatic impedance transforming. *IEEE Trans. Microw. Theory Tech.* **2019**, *67*, 1974–1984. [[CrossRef](#)]
33. Dhar, S.K.; Sharma, T.; Zhu, N.; Darraji, R.; McLaren, R.; Holmes, D.G.; Mallette, V.; Ghannouchi, F.M. Input-harmonic-controlled broadband continuous class-F power amplifiers for Sub-6-ghz 5G applications. *IEEE Trans. Microw. Theory Tech.* **2020**, *68*, 3120–3133. [[CrossRef](#)]
34. Ahn, H.; Tentzeris, M.M. Complex impedance transformers: Their use in designing various ultracompact and wideband power dividers. *IEEE Microw. Mag.* **2020**, *21*, 53–64. [[CrossRef](#)]
35. Nallandhigal, S.N.; Wu, K. Unified and Integrated Circuit Antenna in Front End—A Proof of Concept. *IEEE Trans. Microw. Theory Tech.* **2019**, *67*, 347–364. [[CrossRef](#)]
36. Moghaddasi, J.; Wu, K. Millimeter-Wave Multifunction Multiport Interferometric Receiver for Future Wireless Systems. *IEEE Trans. Microw. Theory Tech.* **2018**, *66*, 1452–1466. [[CrossRef](#)]
37. Gupta, R.; Gabdrakhimov, B.; Dabarov, A.; Nauryzbayev, G.; Hashmi, M.S. Development and Thorough Investigation of Dual-Band Wilkinson Power Divider for Arbitrary Impedance Environment. *IEEE Open J. Ind. Electron. Soc.* **2021**, *2*, 401–409. [[CrossRef](#)]
38. Pozar, D.M. *Microwave Engineering*; John Wiley & Sons: Hoboken, NJ, USA, 2009.
39. Liu, X.; Liu, Y.; Li, S.; Wu, F.; Wu, Y. A three-section dual-band transformer for frequency-dependent complex load impedance. *IEEE Microw. Wirel. Compon. Lett.* **2009**, *19*, 611–613. [[CrossRef](#)]
40. Gupta, R.; Hashmi, M.S.; Maktoomi, M.H. An enhanced frequency ratio dual band balun augmented with high impedance transformation. *IEEE Trans. Circuits Syst. II Exp. Briefs* **2020**, *67*, 2973–2977. [[CrossRef](#)]
41. Maktoomi, M.A.; Hashmi, M.S.; Ghannouchi, F.M. Improving Load Range of Dual-Band Impedance Matching Networks Using Load-Healing Concept. *IEEE Trans. Circuits Syst. II Exp. Briefs* **2017**, *64*, 126–130. [[CrossRef](#)]
42. Monzon, C. A small dual-frequency transformer in two sections. *IEEE Trans. Microw. Theory Tech.* **2003**, *51*, 1157–1161. [[CrossRef](#)]
43. Mousavi, S.M.H.; Rahimi, M.S.; Malakooti, S.A.; Afzali, B.; Virdee, B.S. A broadband out-of-phase gysel power divider based on a dual-band circuit with a single fixed isolation resistor. *Int. J. RF Microw. Comput.-Aided Eng.* **2016**, *26*, 796–802. [[CrossRef](#)]
44. Ren, X.; Song, K.; Fan, M.; Zhu, Y.; Hu, B. Compact Dual-Band Gysel Power Divider Based on Composite Right- and Left-Handed Transmission Lines. *IEEE Microw. Wirel. Compon. Lett.* **2015**, *25*, 82–84. [[CrossRef](#)]
45. Chen, S.; Yu, Y.; Tang, M. Dual-Band Gysel Power Divider with Different Power Dividing Ratios. *IEEE Microw. Wirel. Compon. Lett.* **2019**, *29*, 462–464. [[CrossRef](#)]

Disclaimer/Publisher’s Note: The statements, opinions and data contained in all publications are solely those of the individual author(s) and contributor(s) and not of MDPI and/or the editor(s). MDPI and/or the editor(s) disclaim responsibility for any injury to people or property resulting from any ideas, methods, instructions or products referred to in the content.